Journal of Mechanisms and Robotics

TWO-DIGIT ROBOTIC EXOSKELETON GLOVE MECHANISM: DESIGN AND INTEGRATION

Eric Refour
Robotics and Mechatronics Laboratory
Electrical & Computer Engineering Dept., Virginia Tech
Blacksburg, VA 24060
Email: erefour@vt.edu
ASME Student Member

Bijo Sebastian
Robotics and Mechatronics Laboratory
Mechanical Engineering Dept., Virginia Tech
Blacksburg, VA 24060
Email: bijo7@vt.edu
ASME Student Member

Pinhas Ben-Tzvi[1]
Robotics and Mechatronics Laboratory
Mechanical Engineering Dept., Electrical & Computer Engineering Dept., Virginia Tech
Blacksburg, VA 24060
Email: bentzvi@vt.edu
ASME Member

---

[1] Corresponding author information can be added as a footnote.

1

JMR-17-1307 (Design Innovation), Ben-Tzvi

Journal of Mechanisms and Robotics

Abstract - This paper presents the design and integration of a two-digit robotic exoskeleton glove mechanism. The proposed glove is designed to assist the user with grasping motions, such as the pincer grasp, while maintaining a natural coupling relationship among the finger and thumb joints, resembling that of a normal human hand. The design employs single degree of freedom linkage mechanisms to achieve active flexion and extension of the index finger and thumb. This greatly reduces the overall weight and size of the system making it ideal for prolonged usage. The paper describes the design, mathematical modeling of the proposed system, detailed electromechanical design, and software architecture of the integrated prototype. The prototype is capable of recording information about the index finger and thumb movements, interaction forces exerted by the finger/thumb on the exoskeleton, and can provide feedback through vibration. In addition, the glove can serve as a standalone device for rehabilitation purposes, such as assisting in achieving tip or pulp pinch. The paper concludes with an experimental validation of the proposed design by comparing the motion produced using the exoskeleton glove on a wooden mannequin with that of a natural human hand.

1. INTRODUCTION

Over the past few decades, exoskeletons and haptic gloves have emerged in popularity within the fields of virtual reality (VR) and medical applications. In the realms of VR, exoskeletons and haptic gloves are used to create realistic experiences by generating tactile responses to reflect the sensation of the user touching an object [1–3]. Within the medical field, exoskeleton gloves are used in numerous ways, such as being an assistive tool for tele-operated surgeries or serving as a rehabilitation tool for people who suffer from paralysis in the hand and/or fingers [4–6]. Unfortunately, many of these

2

JMR-17-1307 (Design Innovation), Ben-Tzvi

commercial gloves are expensive and require complex equipment, making them unwieldy

and less portable for activities of daily living (ADLs).

There have been two main approaches for designing exoskeleton gloves

throughout the years. Many researchers use the traditional approach towards building an

exoskeleton glove, which involves using rigid links and joints to apply forces to the

corresponding joints of the human hand to provide assistance with flexion and extension

[7–19]. Most of these exoskeleton gloves are designed with the link frames placed on top

of the fingers and hand instead of alongside the fingers. This is primarily due to the fact

that the size of the link frames exceeds the available space between the fingers. The

major drawback of this concept is that it results in a bulky and heavy glove, which can

result in increased user fatigue during prolonged operation.

The second commonly used approach towards designing exoskeleton gloves is to

replace the rigid mechanisms with softer materials. This approach focusses on using a

tendon-driven design [20–23] or elastic polymers as inflatable membranes, which expand

to achieve the desired bending profiles similar to that of human fingers [24–26].

Unfortunately, both designs have their share of disadvantages. The soft gloves driven by

tendon cables have the following drawbacks: discomfort produced by the pre-tensioning

of the cables, loss in efficiency caused by friction along the tendon path, and the creation

of shear forces applied onto the soft material by the tendons during flexion and extension.

These factors together hinder effective force transmission in tendon driven systems

thereby decreasing their repeatability. On the other hand, the soft inflatable gloves are

challenged by their inability to provide natural flexions and extensions profiles for the

3

JMR-17-1307 (Design Innovation), Ben-Tzvi

human finger and are therefore limited to only achieving the basic configurations of fully

open or closed fist.

The aim of this paper is to present an exoskeleton glove designed to overcome the

previously mentioned drawbacks of traditional rigid and soft exoskeleton gloves. The

exoskeleton glove is intended to be general purpose, possessing the ability to serve as a

medical device or virtual reality haptic glove. As a proof of concept for the proposed

glove design shown in Fig. 1, a two-digit (index finger and thumb) prototype was

developed and its functionality was validated through experimental analysis. For the

experimental analysis, one of the potential applications of the full glove is explored; an

assistive glove providing support for disabled teens/adults. The rest of the paper is

organized as follows: the conceptual design and mathematical modeling are described in

Section 2 while Section 3 covers the detailed electromechanical design of the prototype.

Section 4 presents the integration of the two-digit prototype and Section 5 discusses the

experimental results. Section 6 talks about the possible improvements that can be made to

the design to extend its functionalities by incorporating electric actuation module.
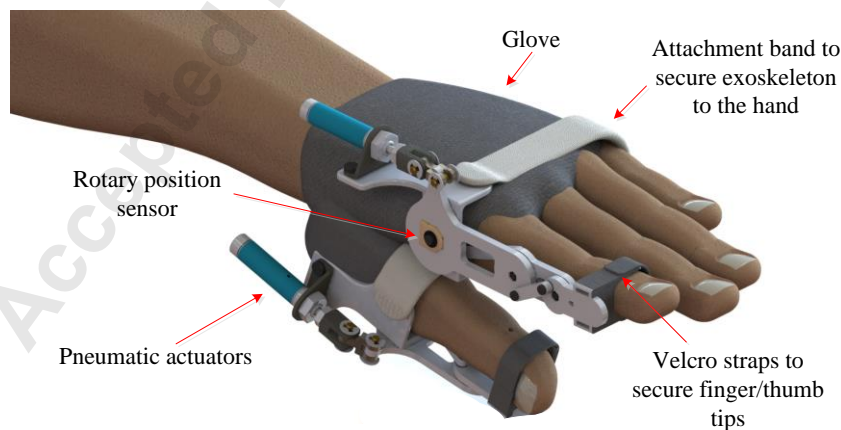
Finally, Section 7 concludes the paper.

Fig. 1 Proposed design

4

JMR-17-1307 (Design Innovation), Ben-Tzvi

2. MECHANICAL DESIGN

In order to overcome the shortcomings of existing systems, the proposed exoskeleton glove was designed to satisfy two primary goals: (1) The weight and size of the total system should be small enough for it to be used in ADL's without fatigue, and (2) The system should be capable of producing natural joint angles on the fingers and thumb during flexion and extension movements.
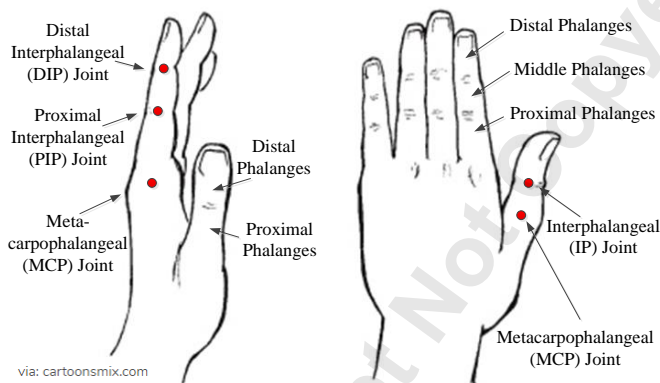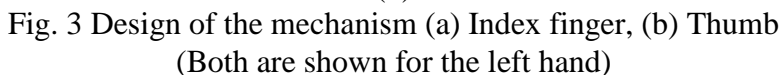

Fig. 2 Anatomy of the human hand

Fig. 2 illustrates the major joints on a human hand. The fingers consist of three main joints, the metacarpophalangeal (MCP), proximal interphalangeal (PIP), and distal interphalangeal (DIP) joints, while the thumb contains the interphalangeal (IP) and MCP joints. In order to design an exoskeleton glove that satisfies the above mentioned goals, existing studies on human grasping motions, such as the common pinch, were reviewed [27–29]. In [30], experiments were performed to measure the joint angles for the index finger and thumb during a tip-pinch motion. The data showed that with a tip-pinch force of 100g and a pulp distance of 1cm, the index finger yielded joint angles of 49.1° (SD 9.5°), 41.0° (SD 10.7°), and 38.5° (SD 6.8°) for the MCP, PIP, and DIP joints respectively while the thumb yielded 12.8° (SD 9.4°), and 21.8° (SD 7.8°) for the MCP and IP joints. This data was used as a reference to design the exoskeleton glove.

5

JMR-17-1307 (Design Innovation), Ben-Tzvi

Journal of Mechanisms and Robotics

A major conclusion drawn from these studies is the existence of inherent coupling of the human finger (MCP, PIP and DIP joints) and thumb (IP and MCP joints). As a result of this coupling, the human fingers and thumbs essentially behave as single DOF systems while flexing and extending to perform common grasping motions. Making use of this factor in the design reduces the number of actuators needed, which in turn reduces the overall size and weight of the system.

The conceptual design for the proposed glove is inspired from the USC/Belgrade Robotic Hand [31]. The coupling mechanism used in this robotic hand was proven successful, so the approach was to adopt a similar coupling mechanism and modify it for suitable use in an exoskeleton glove. The proposed design for the glove mechanism consists of planar links that are connected by revolute joints, as detailed in Fig. 3.

(a)

(b)

Fig. 3 Design of the mechanism (a) Index finger, (b) Thumb
(Both are shown for the left hand)

6

JMR-17-1307 (Design Innovation), Ben-Tzvi

The basic structure of the mechanism for the index finger is composed of links L_1, L_2, and L_3, which correspond to the proximal, middle, and distal phalanges of the finger respectively, as shown in Fig. 3. These three links are connected through three revolute joints, R_1, R_2, and, R_3. Specifically, links L_i and L_{i+1} are connected through revolute joint R_{i+1}. The constraint links C_1 and C_2 are used to produce the coupling relationship between the L_i links. Constraint link C_1 connects link L_2 to a fixed base frame (ground) by revolute joints Rc_1 and Rc_2, while constraint link C_2 connects links L_1 to L_3 through joints Rc_3 and Rc_4. The thumb mechanism is similar, containing only links L_1 and L_2, which are connected by revolute joint R_2. The coupling action for the thumb mechanism is achieved by the constraint link C_1, which connects link L_2 to the base frame through the revolute joints Rc_1 and Rc_2. The assembly of the mechanisms shown in Fig. 3 can be summarized in the following steps:

- Link L_1 is connected to the ground at joint R_1
- Link L_1 is connected to link L_2 at joint R_2
- Link L_2 is connected to link L_3 at joint R_3 *
- Constraint link C_1 connects to the ground at constraint joint Rc_1 and to link L_2 at constraint joint Rc_2
- Constraint link C_2 connects to link L_1 at constraint joint Rc_3 and to link L_3 at constraint joint Rc_4 *

Note: * only applied for the finger mechanism and not for the thumb mechanism.

The flexion and extension motions are achieved when a rotary motion is applied at joint R1 by pushing and pulling on the lever of link L_1 respectively. This causes link L_1 to bend and as it bends, the constraint links C_1 and C_2 translates the motion along to links L_2 and L_3, as illustrated in Fig. 4. This collectively provides the coupling motion that reflects the natural flexion and extension of a human finger.

7

JMR-17-1307 (Design Innovation), Ben-Tzvi

2.1 Kinematic Modeling

Before a detailed mechanical design of the exoskeleton glove could be created,

the lengths of various links and positioning of revolute joints had to be determined based

on the general dimensions of a human hand and the joint angles desired to be achieved in

reference to [30]. To this extent, a kinematic modeling of the mechanism was performed.

The modelling was done by taking into consideration the following design parameters

(illustrated in Fig. 4):

- l_i- length of link L_i, measured as the normal distance from R_i to R_{i+1}. For l_3, the distance is measured from R3 to the tip of the end-effector/L3
- c_i- length of constraint link C_i, measured as the normal distance from Rc_i to Rc_{i+1}
- θ_i- joint angle of link L_i, defined as the angle measured from the x-axis of the base coordinate frame to the x-axis of the body coordinate frame
- d_i- the radial distance from constraint joint Rc_i to the origin of the corresponding link body coordinate frame
- φ_i- the angle made by constraint joint Rc_i with respect to the vertical y-axis of the body coordinate frame for link L_i, measured in the counter-clockwise direction (*Note: φ_2 and φ_4 are measured from the positive y-axis, while φ_1 and φ_3 are measured from to the negative y-axis*)
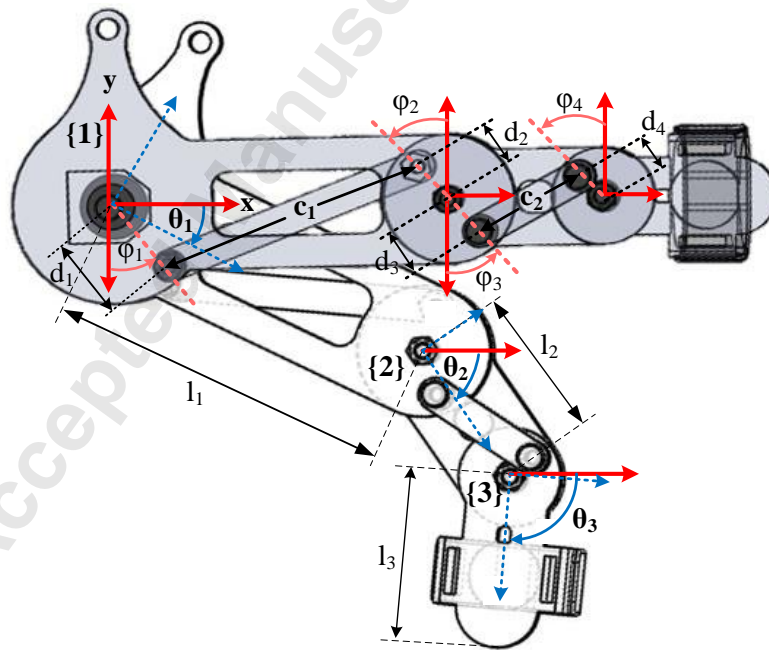

Fig. 4 Index mechanism showing two configurations and the design parameters for kinematic modelling. The relaxed configuration is shown in gray, while the black and white schematic shows a flexion configuration.

8

JMR-17-1307 (Design Innovation), Ben-Tzvi

Journal of Mechanisms and Robotics

The finger mechanism has three planar links with body coordinate frames attached to the joint, which are defined as $[\,(x_1, y_1, \theta_1), (x_2, y_2, \theta_2), (x_3, y_3, \theta_3)\,]$. The location of each link is represented by the x_i and y_i terms, while the θ_i terms reflect the joint angles produced by the flexion/extension motions. These joint angles are measured from the x-axes of the original base coordinate frames of the links to the x-axes of the new body coordinate frames, which result from the mechanism being in motion. The base coordinate frame is illustrated in Fig. 4 by red coordinate lines (x, y), while the body coordinate frames are shown by the blue dotted lines. All of the coordinate frames are right handed, with the z-axes pointing forward (out of the page).

The thumb mechanism on the other hand has two links, which are defined by the coordinates $[\,(x_1, y_1, \theta_1)\,,\,(x_2, y_2, \theta_2)\,]$. For the single DOF mechanism for the index finger, establishing θ_1 as the input variable in the modeling yields the following eight constraint equations:

$$x_1 = 0$$

$$y_1 = 0$$

$$x_2 = x_1 + l_1 \cos \theta_1$$

$$y_2 = y_1 + l_1 \sin \theta_1$$

$$x_3 = x_2 + l_2 \cos \theta_2 \qquad\qquad (1)$$

$$y_3 = y_2 + l_2 \sin \theta_2$$

$$c_1^2 = [x_2 - (d_2 \sin \varphi_2 \cos \theta_2 + d_2 \cos \varphi_2 \sin \theta_2) - d_1 \sin \varphi_1]^2$$
$$\quad + [y_2 + (d_2 \cos \varphi_2 \cos \theta_2 - d_2 \sin \varphi_2 \sin \theta_2) + d_1 \cos \varphi_1]^2$$

9

JMR-17-1307 (Design Innovation), Ben-Tzvi

$$
\begin{aligned}
c_2^2 = &\ [(x_3 - (d_4 \sin \varphi_4 \cos \theta_3 + d_4 \cos \varphi_4 \sin \theta_3)) \\
&\ - (x_1 + (l_1 + d_3 \sin \varphi_3) \cos \theta_1 + d_3 \cos \varphi_3 \sin \theta_1)]^2 \\
&+ [(y_3 + (d_4 \cos \varphi_4 \cos \theta_3 - d_4 \sin \varphi_4 \sin \theta_3)) \\
&\ - (y_1 + (l_1 + d_3 \sin \varphi_3) \sin \theta_1 - d_3 \cos \varphi_3 \cos \theta_1)]^2
\end{aligned}
$$

For the above equations, the constraint links C_i are considered to be absolute distance constraints. For the kinematic model, the link lengths L_i were set to general dimensions of a human hand. The other design parameters were estimated using a MATLAB simulation so that the joint angles achieved by the mechanism matched with the joint angles of a natural human finger. The design procedure for the thumb mechanism follows the same steps, but with only two main links L_i and one constraint link C_i. For the simulations, the joint angles were measured using the following relationships: (i) MCP joint = θ_1, (ii) PIP joint (IP for thumb) = $\theta_2 - \theta_1$, and (iii) DIP joint = $\theta_3 - \theta_2$.
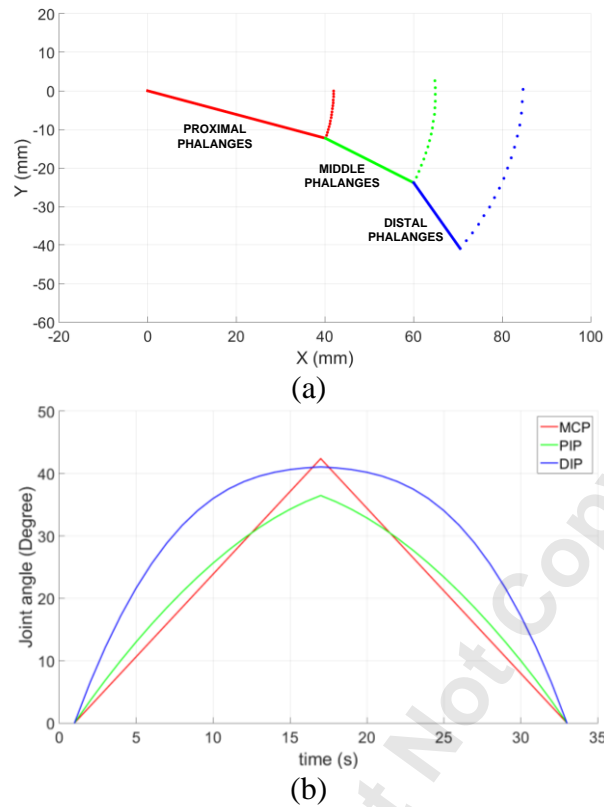
10

JMR-17-1307 (Design Innovation), Ben-Tzvi

Journal of Mechanisms and Robotics

(a)

(b)

Fig. 5 Simulation results (a) Desired index finger trajectory starting at the origin of (0, 0), (b) Index finger joint angles.

11

JMR-17-1307 (Design Innovation), Ben-Tzvi

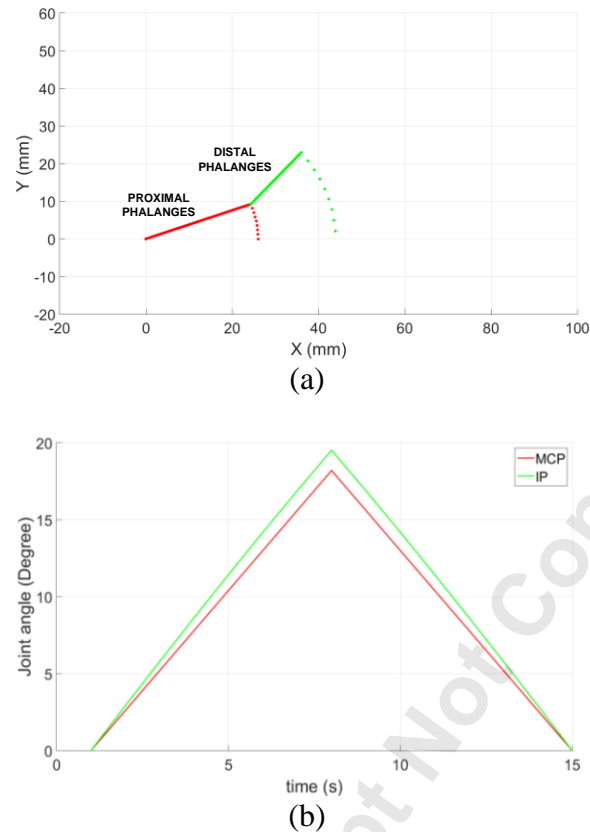Journal of Mechanisms and Robotics

(a)

(b)

Fig. 6 Simulation results (a) Desired thumb trajectory starting at the origin of (0, 0), (b) Thumb joint angles.

Fig. 5 and Fig. 6 each present the kinematic simulation results using the estimated design parameters. For both simulations, the angles produced were negative, but for the sake of visualization, they are plotted as positive values. The index finger trajectory can provide maximum angles of 43°, 41°, and 37° for the MCP, PIP, and DIP joints respectively, while the thumb trajectory offers MCP and IP angles of 19° and 17° respectively. The simulated trajectories reflect the natural joint relationship of the index finger and thumb during the 100g tip-pitch motion, shown in Fig. 5a and Fig 6a respectively. These modelling results confirm that the each mechanism is capable of enforcing joint angles resembling that of a natural human hand.

12

JMR-17-1307 (Design Innovation), Ben-Tzvi

Journal of Mechanisms and Robotics

3. ELECTRO-MECHANICAL DESIGN

3.1 Actuation

To achieve flexion and extension motions with adequate speed and force, Bimba double acting pneumatic actuators were used for the index finger and thumb mechanisms of the exoskeleton glove. With these actuators, the glove can complete flexion and extension motions within 1s with a force of 10N. The complete pneumatic system consists of an air compressor (150 PSI), a 0.5 gallon air reservoir, a pressure regulator, air tubing, and solenoid valves by SMC Corporation, which control the air flow into the pneumatic actuators.

3.2 Sensors

For absolute position sensing, Bourns rotary encoders were placed on each of the finger and thumb mechanisms at the R_1 joints, which correspond to the MCP joints on the human hand. The readings from the electrical encoders correspond to the angular position of the L_1 links of the finger and thumb mechanisms. A digital protractor was used to manually calibrate the encoder values into angle measurements. The remaining joint angles of the PIP and DIP joints of the index finger and the IP joint of the thumb are calculated using the kinematic model of the mechanism. Using the kinematic model, the position of the final link that corresponding to the distal phalanges of the finger and thumb can also be calculated.

Force sensitive resistors (FSR) by Interlink Electronics were used to measure the amount of force being applied on the index finger and thumb by the exoskeleton frames during grasping. These FSR sensors have a continuous analog resolution and a force sensitivity range of 0.2N – 20N. Two force sensors are placed on each of the

13

JMR-17-1307 (Design Innovation), Ben-Tzvi

Journal of Mechanisms and Robotics

finger/thumb tip pieces, as shown in Fig. 7. The force sensors were calibrated using known weights.
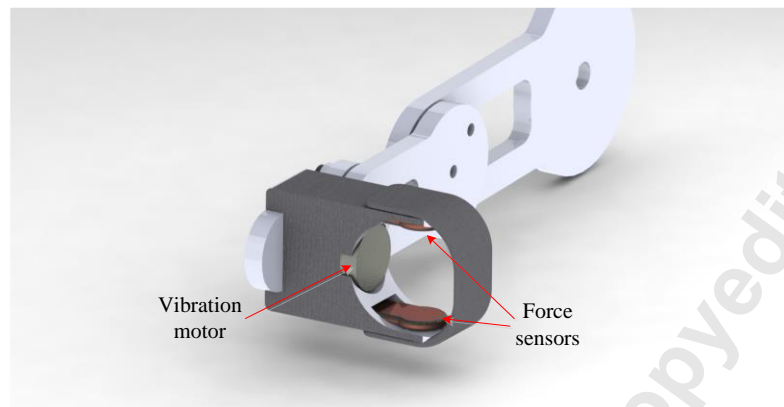

Fig. 7 Design of the tip holder shown on finger mechanism
(same for thumb mechanism)

In addition to the sensors, vibration motors were added to the design in order to provide feedback to the user. This feedback can be used in several applications such as, providing haptic feedback for virtual reality applications, acting as a stimulus to prompt the user to perform certain tasks for rehabilitation, or as feedback for tele-navigation [3]. The motors used were Adafruit mini vibration motors, which are rated for 5V max with a current draw of 100mA. The motors have a weight of 0.9 grams and can provide a vibration sensation that resembles that of a standard mobile phone vibrating unit.

4. PROTOTYPE INTEGRATION

The basic mechanisms shown in Fig. 3 were further developed into a detailed design for the two-digit prototype. The detailed design of the system is shown in Fig. 1. The mechanisms for the index finger and the thumb were 3D printed separately using ABS plastic and then connected together using a base plate. The base plate, which supports the weight of the two mechanisms and the actuators, was strapped onto the back

14

JMR-17-1307 (Design Innovation), Ben-Tzvi

of the hand using elastic Velcro straps. This allows for the adjustment of the exoskeleton

glove to suit different hand sizes. The prototype weighs 24g, making it lightweight as

compared to the two finger exoskeleton of [32], which weighs 180g. To complete the

prototype implementation, a circuit board and software interface were developed to

control the glove and all integrated sensors. The circuit board and pneumatic system were

kept separate so that they could be either incorporated into a backpack or kept on a table

while the exoskeleton glove was being used.

4.1 Electrical Circuit

A custom printed circuit board (PCB) was developed to connect the sensors and

actuators with the microcontroller unit and other electrical components. The force sensors

and encoders were connected to the microcontroller unit as inputs while the pneumatic

actuators and vibration motors were the output connections. The pneumatic actuators

were controlled using the solenoid valves to produce a linear actuation. The

microcontroller itself powers these solenoid valves on/off via N-MOSFET switches. The

vibration motors are directly connected to a motor driver since the current ratings of these

motors exceed the tolerance of the microcontroller input/output (I/O) pins. The

microcontroller connects to the motor driver with two enable pins for each vibration

motors, one for the index finger and another for the thumb.

A Teensy 3.1 board serves as the microcontroller unit for the system. It is rated at

a clock frequency of 72 MHz, which provides sufficient speed for acquiring sensor data

from the encoders and force sensors while performing commands to control the vibration

motors and the actuation for flexion or extension of the index and thumb.

15

JMR-17-1307 (Design Innovation), Ben-Tzvi

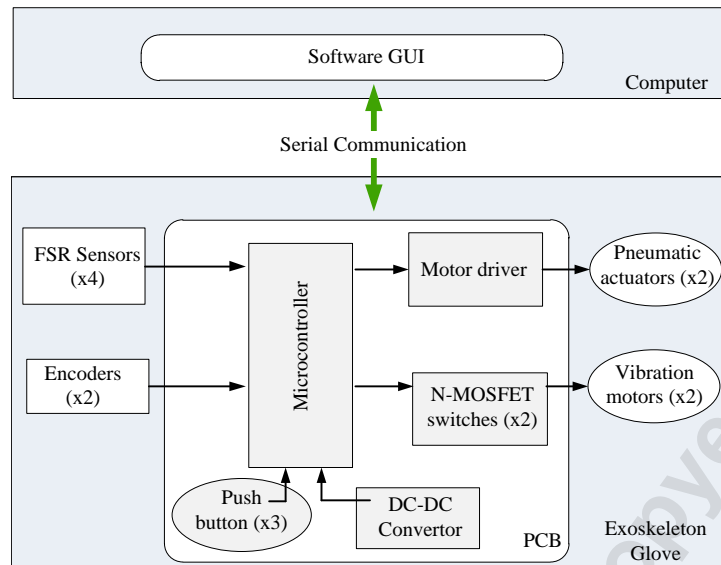Journal of Mechanisms and Robotics

Fig. 8 System architecture of exoskeleton glove

In addition to the sensors and motors, the PCB contains three tactile pushbuttons. One pushbutton serves as the main power switch while the other two are used for actuation controls. One of these two is used to depressurize the pneumatic actuators to allow free movements among the finger and thumb. The last button is used to trigger an automatic flexion and extension motion on both the finger and thumb to perform a grasp. This feature allows the exoskeleton device to serve as a standalone device for different applications such as rehabilitation. For full feature controls, the PCB can be interfaced with the Graphical User Interface (GUI) for the exoskeleton glove system that provides additional commands and functionalities. The overall architecture of the exoskeleton glove system is demonstrated in Fig. 8.

4.2 Software GUI

The Exoskeleton GUI is an executable application developed in MATLAB. This software provides additional commands to control the glove and functionalities for data analysis. To control the glove actuation, the commands are divided into the following

16

JMR-17-1307 (Design Innovation), Ben-Tzvi

groups: index finger controls, thumb controls, and both the index finger and thumb together. Each of these control groups consists of the following commands to control only the specified finger/thumb: Trigger Motion, Release, and Vibrate Pulse. The Index and Thumb combined control group contains these same commands as well as additional commands such as the Auto Trigger and Release Pinch command, which actuates the index finger and thumb to perform a pincer grasp and then releases the pinch after a time delay of 1.50s. For all three control groups, the Vibrate Pulse commands were programmed to turn on the corresponding vibrate motors for 0.5s. The GUI commands for actuating the pinching motions for each digit is accomplished by signaling the microcontroller to power the solenoid valves on and off accordingly, as mentioned in Section 4.1.

While reading in the sensor data, the GUI displays the FSR sensor data in terms of Newtons (N) and the encoder data in degrees for both the index and thumb. For analysis purposes, the GUI has a record feature that will capture sensor data at a rate of 20Hz and store the data into a Microsoft Excel file. An additional feature of the GUI includes an imported SolidWorks CAD model of a human hand. The CAD model was incorporated to serve as a real-time animation showing the movements of the user's hand while using the glove.

5. EXPERIMENTAL VALIDATION

An experiment was conducted to verify whether the joint angles enforced on the index finger and thumb by the glove during flexions and extensions reflect the desired trajectories for obtaining natural joint coupling. The experiment involved mounting the exoskeleton glove on a wooden mannequin hand and tracking the motions of index finger

17

JMR-17-1307 (Design Innovation), Ben-Tzvi

Journal of Mechanisms and Robotics

and thumb, which were produced by the glove, as shown in Fig. 9. The tracking was achieved using a GoPro HERO5 Session 10MP camera with 4K video resolution. To capture the finger and thumb at various stages during motions, the camera was set up to record videos at 30 frames per seconds (FPS). A MATLAB script was programmed to utilize basic computer vision techniques to analyze the captured images. The code first identifies red markers placed on the MCP, PIP, and DIP joints and MCP and IP joints of the inserted index finger and thumb respectively. Once these red markers were identified, the centroids of the markers were computed to determine the centers of the joints. Line segments were drawn between the joint centers such that the corresponding joint angles could be calculated (illustrated in Fig. 10). Thus from identifying the red markers from image to image, the overall joint angles were calculated and used to analyze the joint coupling relationships enforced by the exoskeleton glove.
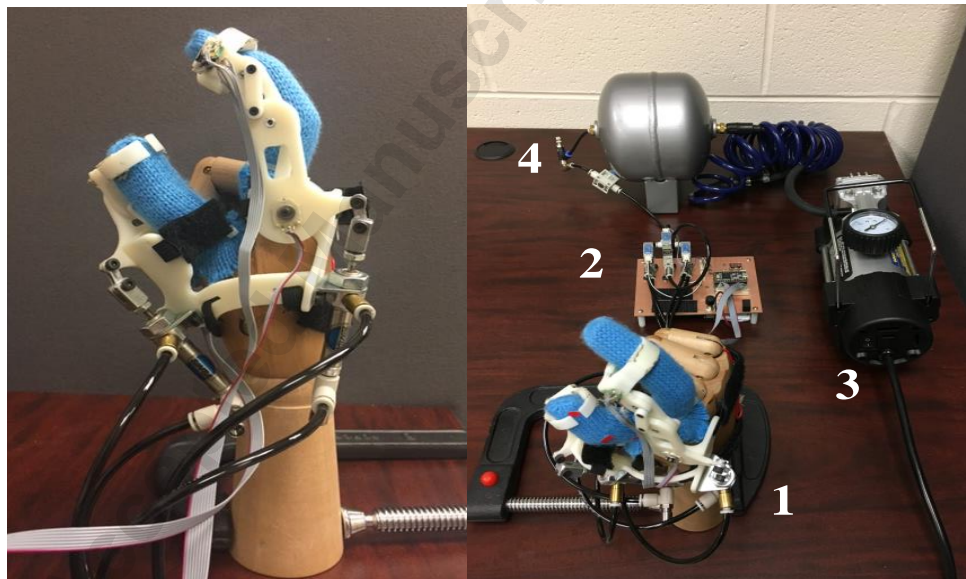

Fig. 9 Experimental setup for the prototype: 1- Exoskeleton glove on mannequin, 2 - Embedded controller, 3 – Compressor, 4 - Air tank

18

JMR-17-1307 (Design Innovation), Ben-Tzvi

Although the GoPro camera is equipped with an ultra-wide angle lens that has reduced distortion, it was still necessary to apply a distortion correction filter to each of the video image frames prior to the joint tracking procedure. In order to accomplish this, a camera calibration was performed using the traditional method of capturing several pictures of a standard checkerboard pattern using the subject camera [33]. The distorted images of the checkerboard were then analyzed using the MATLAB camera calibration toolbox to compute the camera intrinsic, extrinsic, and lens-distortion parameters. These parameters were used for the undistortion filtering.

To overcome the lack of inherent coupling between the respective thumb and index finger joints of the mannequin hand, the index finger and thumb were inserted into a cloth glove as shown in Fig. 10. This allows for the joints to bend in correlation, when the mechanisms for index finger and thumb apply force at the distal phalange of the corresponding finger/thumb.

Fig. 10 Experimental analysis at various stages of the bending motion: (a) Index finger, (b) Thumb

19

JMR-17-1307 (Design Innovation), Ben-Tzvi

Journal of Mechanisms and Robotics

The experiment for each digit was performed independently of one another. The results from these experiments are plotted in Fig. 11, which displays the calculated joint angles for both digits with respect to time. The MCP, PIP and DIP joints of the index finger bend at average angle of 42.9°, 37.8°, and 8.01° respectively, while the MCP and IP joints of the thumb respectively bend 3.01° and 22.5°. To verify the coupling relationships of the joints, the results were compared to the targeted natural angles from [30], which were previously mentioned in Section 2. Fig. 11 displays the comparisons by plotting the resulting joint angles against the acceptable ranges of the natural joint angular displacements. More specifically, the experimentally derived upper and lower bounds for the natural joint angles for a tip-pinch force of 100g (1cm pulp distance) were computed by adding and subtracting the standard deviation with the joint angle averages [30]. These upper and lower boundaries serve as the range of acceptable variations for each of joint angle maximums.

As seen from Fig. 11, the angular displacements for the MCP and PIP joints of the index finger were well within their acceptable range for natural angular displacements at the end of the pinch. However, the final angular displacement for the DIP joint of the index finger fell short from reaching within its perspective boundary by 23.7°. The MCP angular joint displacement for the thumb fell within its range while the IP joint was on the boundary of the acceptable range, falling short by 0.4°.

20

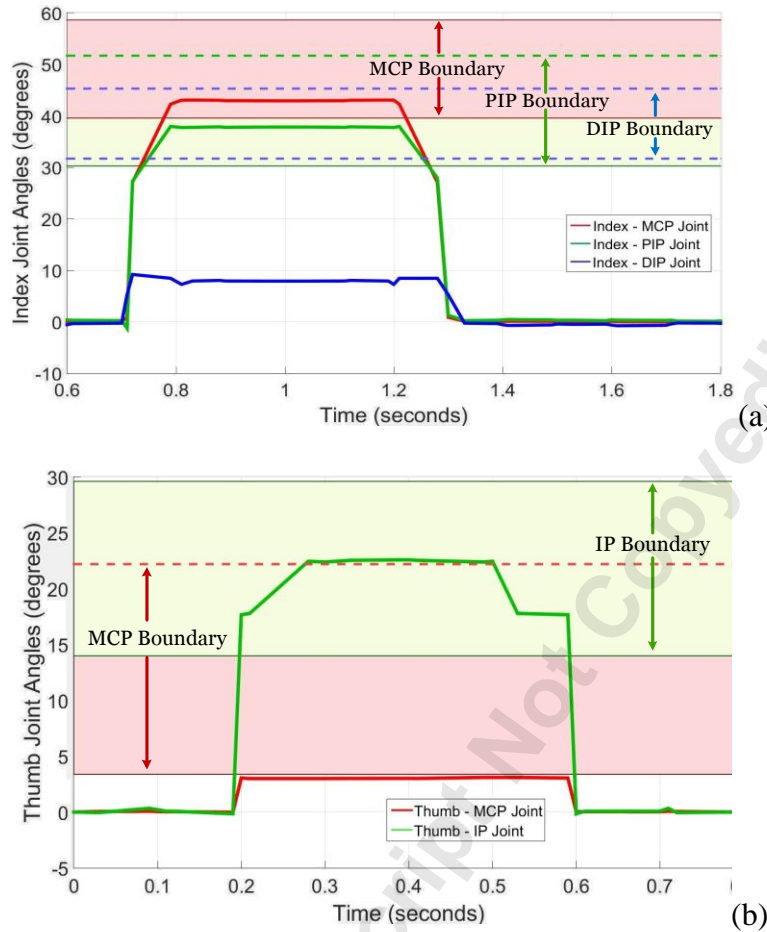JMR-17-1307 (Design Innovation), Ben-Tzvi

Fig.11 Experimental results for (a) Index finger joints,
(b) Thumb joints

The shortcoming of the index finger DIP joint angle was due to the misalignment

of the Velcro fingertip holder. Instead of being positioned at the distal phalange region of

the mannequin hand, the holder was located near the DIP joint. This misalignment was

due to the size difference between the mannequin hand and the human hand, for which

the holder piece was originally designed to accommodate. The mannequin fingers were

longer (index finger by 3cm and thumb by 1cm) than that of an average human hand and

as a result, the mechanism was able to slide down the mannequin finger during the

bending movements of the experiment. The same reason applies to the IP joint angles of

21

JMR-17-1307 (Design Innovation), Ben-Tzvi

Journal of Mechanisms and Robotics

the thumb coming short of the acceptable range. The glove can be seen properly worn on
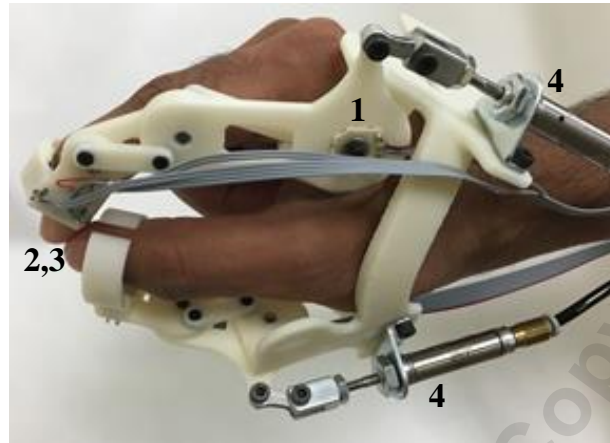
a human hand in Fig. 12.

Fig. 12 Prototype on a human hand: 1- Absolute position
sensor, 2 - FSR sensor, 3 - Vibration motor, 4 - Pneumatic
actuator

Overall, the pincer grasp was achieved in 0.63 seconds, with 0.1 seconds for the

pinch, 0.41 seconds to hold the pinch, and another 0.12 seconds for releasing. Despite the

experimental shortcoming of the DIP joint of the index finger, the results demonstrated

that the joint angles produced by the exoskeleton resemble natural bending trajectories of

the human hand during grasping motions, such as the pincer grasp.

6. DESIGN IMPROVEMENTS AND FUTURE WORK

6.1 Motivation

Although the proposed design produced promising results in being a lightweight

hand exoskeleton that can emulate natural joint angles, improvements will be needed to

expand this proof of concept into a fully functional assistive device that would be

sufficient for ADLs. Some of these shortcomings are listed below:

22

JMR-17-1307 (Design Innovation), Ben-Tzvi

- Actuation: Even though the pneumatic actuation method offers speed and power, it lacks the ease of controllability. Specifically, pneumatic actuators naturally allow for two basic configurations: full flexion and full extension of the hand exoskeleton digits (fully open glove and fully closed). To allow for efficient grasping of the various objects that humans interact with daily, the hand exoskeleton must have the ability to conform to the shape of the object being grasped. This therefore requires the actuation system to be able to achieve any of the infinite configurations between the range of maximum flexion and maximum extension.

- Force Feedback: With the human hand being a complex structure with many capabilities, it can offer a variety of grasps and pinches. These grasps differ according to the joint angles, trajectories, and orientations of the fingers and thumb and the overall output grip force. To control various grasps at high precision when interacting with objects or completing tasks, the human hand incorporates sensory processing with its motor skills. This allows the human hand to receive force feedback across many nerves within the hand at high level of sensitivity and react accordingly. Although the proposed design contains force sensors that can measure interactive forces, it lacks the ability to use this force information as feedback input for controlling the force, speed, and ending trajectories of each finger and thumb of the hand exoskeleton. Without the hand exoskeleton having this type of compliance functionality, it will not be able to adjust the strength of its grasp and finger trajectories.

- Portability: When designing a hand exoskeleton that can primarily serves as an assistive glove or as a haptic device, portability becomes a major design parameter.

23

JMR-17-1307 (Design Innovation), Ben-Tzvi

The use of a pneumatic actuation system does not achieve this design goal however. As shown in Fig. 9, pneumatic actuators require items such as an air tank and compressor to create a fully functional system, which are not ideal to carry around for an extended period of time. Another solution may be to have a smaller air tank and compact compressor that could fit inside a backpack for the user to wear, thus making the pneumatic system portable. Despite this being a plausible approach, it creates the concerns of having less available air for the pneumatic actuators to use between refills and adds more weight for the user to carry, thereby introducing serious issues for the elderly and disabled. As a proof of concept for the proposed designed, the pneumatic actuation was sufficient for experimental validation. But for a portable system the actuation system has to be redesigned possibly with miniature light weight DC motors powered by LiPo batteries.

In order to address the shortcomings of the proposed design, future versions of the prototype will replace the pneumatic actuation system with electrical actuators using a series elastic actuator (SEA) design. SEAs are commonly used to achieve force control in robotic systems that interact with the environment. SEAs can be implemented by placing an elastic element, such as a torsional or compression spring in series between the drive train of an actuator and its payload, thereby creating a compliant actuation unit. In addition to being essential for the SEA design, the use of electrical actuators in place of the pneumatic system makes the system more portable. By shifting towards an electrical actuation system, the hand exoskeleton will be able to achieve desired forces and speeds while being powered by lightweight and high energy density LiPo batteries. In the section

24

JMR-17-1307 (Design Innovation), Ben-Tzvi

Journal of Mechanisms and Robotics

below, the motivation for SEAs is explained and the proposed design is presented in detailed.

6.2 SEA Design

An ideal actuation unit for a force controllable robotic system is one that can perfectly output the desired force, regardless of any inertia produced from the movement of the payload. Despite the advancement in technology, modern actuators possess several limitations that hinder them from being perfect candidates for force control. Some of these limitations includes: mechanical impedance, stiction friction, and low actuator mechanical bandwidth [34]. Impedance in the actuator is due to the inertia or additional forces that are created by the load motion. This force is reflected onto the overall output force from the actuator, which can introduce errors in efficiently achieving the desired force. Like many other robotic systems, the proposed design contains several mechanical components that slide against each other. This sliding behavior results in stiction friction. In order to overcome the resistance due to stiction friction, the actuator has to exert a higher breakaway force, which in return limits the minimum force the actuator can output. This in turn leads to the issue of low bandwidth due to the mechanical stiffness and power saturation of the actuation module.

SEAs serve to overcome these issues due to the elasticity factor which allows for storing energy while also introducing shock tolerance within the system. Not only does it help with making the system more compliant with the environment, but the tolerance also allows for the actuation unit to be more back drivable. As a result, this lowers the amount of impedance in the system and the mechanical stiffness that negatively impacts the force bandwidth. Most importantly, SEA offers a way to achieve force control by means of

25

JMR-17-1307 (Design Innovation), Ben-Tzvi

primarily controlling position using Hooke's Law [34], [35]. In most cases, position is easier to control accurately in motors that use gear trains or have feedback encoders attached. Overall, SEAs utilize active sensing and closed loop controls to reduce the disturbances from friction and inertia to ultimately achieve the desired force output.

The design of the proposed SEA is detailed in Fig. 13. The design uses a geared DC motor with a leadscrew acting as the shaft. The geared DC motor offers a high torque, at sufficiently low speed. The leadscrew shaft allows for the translation of rotary motion into linear motion, reflecting the original linear drive of the pneumatic actuators. The design was adapted from the traditional SEA design done by [34]. The overall actuation unit consists of three major components: a drive-train, output carriage, and compression springs. The drive-train component houses a ball nut that attaches to the leadscrew shaft, allowing the entire drive-train unit to move forward and backwards along the shaft as the motor rotates clockwise and counter-clockwise, respectively. The drive-train component is coupled with the output carriage unit by the placement of compression springs between both components. Specifically, the drive-train component is placed between both ends of the output carriage unit. A compression spring is placed on each side of the drive-train, establishing springs between the drive-train and output carriage on both sides. Therefore, as the drive-train component moves forward and backward along the leadscrew, the compression springs push and pull against the output carriage component, causing it to move in synchronization with the drive-train component. The overall output force from the leadscrew motor and compression springs is reflected onto the output carriage unit. This force on the output carriage is used to push

26

JMR-17-1307 (Design Innovation), Ben-Tzvi

the lever of the finger/thumb mechanism. To align all of the components together during

motion, a guide rail is installed above the leadscrew shaft.
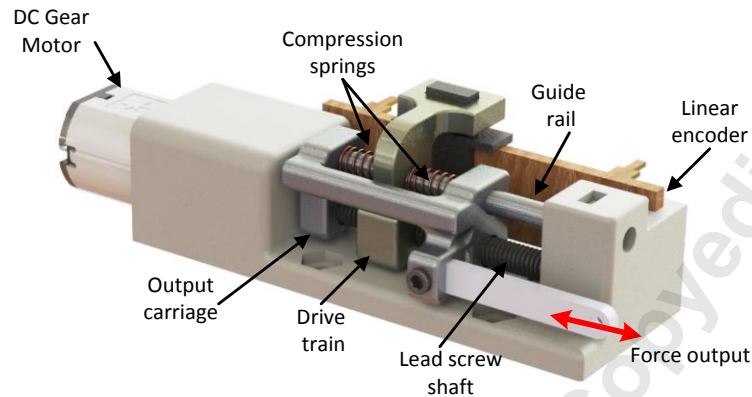

Fig.13 Proposed SEA design

During operation, the output forces can be measured through the deflection of the

compression springs. To measure the spring deflection, a linear encoder is incorporated

into the SEA design by attaching the scale of the encoder onto the drive-train component,

as shown in Fig. 13. This attachment allows the scale of the encoder to move in

accordance with the drive-train for tracking its position. Using the absolute rotary

encoders that are placed onto the glove mechanisms at the MCP joint of the fingers and

thumb, the position for the output carriage piece can also be tracked. As a result, the

deflection of the springs can be calculated using the positioning information for both the

drive-train and the output carriage components. By optimizing the stiffness of the springs,

the desired force bandwidth and sensitivity can be attained from the SEA unit [34]. A

prototype of the proposed SEA design was 3D printed and is shown in Fig. 14. By

equipping both the index finger and thumb mechanism of the proposed hand exoskeleton

with the SEA actuation unit as shown in Fig. 15, the exoskeleton glove will be able to

27

JMR-17-1307 (Design Innovation), Ben-Tzvi

grasp objects of various shapes and strengths while maintaining a stable grip through force control.
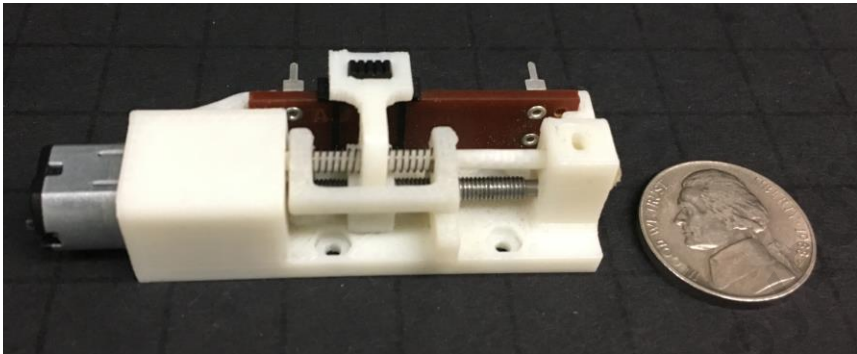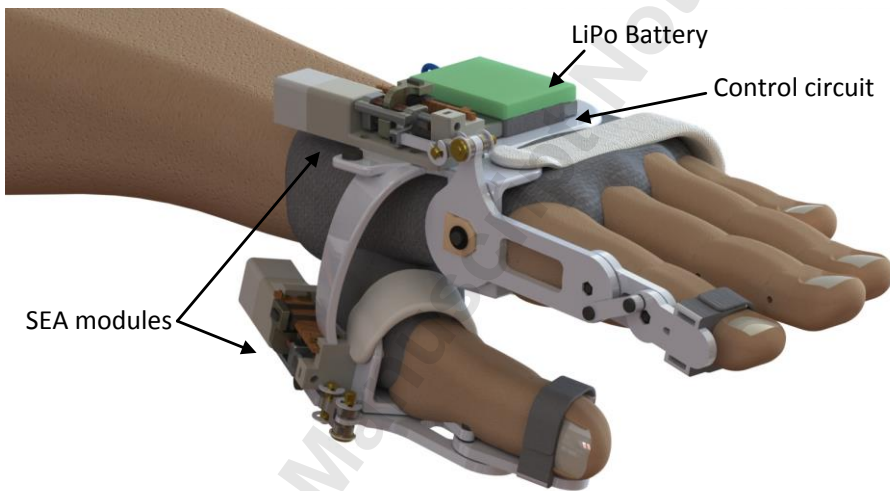

Fig. 14 3D printed prototype of the SEA module

Fig. 15 Proposed Exo-Glove design with electric actuation and SEA

7. CONCLUSION

The paper presented the design and integration of a two-digit prototype of an exoskeleton glove that was proposed to address the commonly encountered large size, heavy weight, and unnatural coupling issues of traditional hard and soft exoskeleton gloves. The design of the exoskeleton glove allows for the finger and thumb mechanisms to be attached alongside the respective finger/thumb, decreasing the size of the

28

JMR-17-1307 (Design Innovation), Ben-Tzvi

Journal of Mechanisms and Robotics

exoskeleton glove as well as reducing the discomfort caused from using larger and heavier traditional gloves. Mathematical modeling of the design was presented and the proposed concept was validated through experiments. Results showed the potential of the exoskeleton glove to achieve natural coupling among the joints to resemble that of a human hand. Although the initial features of the prototype to record finger and thumb movements, measure exerted forces on the glove, and provide vibrational feedback, make it suitable for multiple applications, the pneumatic actuators present several shortcomings that affect performance. These shortcomings were analyzed and a feasible solution was presented, which proposed using SEAs as alternative actuation methods. The proposed SEA design was further developed into a proof-of-concept prototype.

Future work will involve implementing force feedback and control with the proposed SEA prototype. In addition, the two-digit design will be extended into a full hand exoskeleton glove by modifying the index finger mechanism to accommodate for the additional fingers. The overall grasping performance with force control will be investigated using the full hand exoskeleton glove.

29

JMR-17-1307 (Design Innovation), Ben-Tzvi

REFERENCES

[1]   "MANUS VR," 2014. [Online]. Available: manus-vr.com. [Accessed: 14-Sep-2017].

[2]   CyberGlove Systems LLC, "CyberGrasp," 2009. [Online]. Available: http://www.cyberglovesystems.com/cybergrasp/. [Accessed: 14-Sep-2017].

[3]   H. Tatsumi, Y. Murai, I. Sekita, S. Tokumasu, and M. Miyakawa, "Cane Walk in the Virtual Reality Space Using Virtual Haptic Sensing: Toward Developing Haptic VR Technologies for the Visually Impaired," *Proc. - 2015 IEEE Int. Conf. Syst. Man, Cybern. SMC 2015*, pp. 2360–2365, 2016.

[4]   S. Ito, H. Kawasaki, Y. Ishigure, M. Natsume, T. Mouri, and Y. Nishimoto, "A design of fine motion assist equipment for disabled hand in robotic rehabilitation system," *J. Franklin Inst.*, vol. 348, no. 1, pp. 79–89, 2011.

[5]   C. D. C. Teixeira, F. C. Marx, and J. C. De Oliveira, "A Haptic Rehabilitation System," *Proc. - 18th Symp. Virtual Augment. Reality, SVR 2016*, pp. 188–192, 2016.

[6]   P. Heo, G. M. Gu, S. jin Lee, K. Rhee, and J. Kim, "Current hand exoskeleton technologies for rehabilitation and assistive engineering," *Int. J. Precis. Eng. Manuf.*, vol. 13, no. 5, pp. 807–824, 2012.

[7]   Z. Ma and P. Ben-Tzvi, "Tendon transmission efficiency of a two-finger haptic glove," *ROSE 2013 - 2013 IEEE Int. Symp. Robot. Sensors Environ. Proc.*, no. October, pp. 13–18, 2013.

[8]   N. S. K. Ho *et al.*, "An EMG-driven exoskeleton hand robotic training device on chronic stroke subjects: Task training system for stroke rehabilitation," *IEEE Int. Conf. Rehabil. Robot.*, 2011.

[9]   J. Iqbal, H. Khan, N. G. Tsagarakis, and D. G. Caldwell, "A novel exoskeleton robotic system for hand rehabilitation - Conceptualization to prototyping," *Biocybern. Biomed. Eng.*, vol. 34, no. 2, pp. 79–89, 2014.

[10] J. Arata, K. Ohmoto, R. Gassert, O. Lambercy, H. Fujimoto, and I. Wada, "A new hand exoskeleton device for rehabilitation using a three-layered sliding spring mechanism," *Proc. - IEEE Int. Conf. Robot. Autom.*, pp. 3902–3907, 2013.

[11] T. T. Worsnopp, M. A. Peshkin, J. E. Colgate, and D. G. Kamper, "An actuated finger exoskeleton for hand rehabilitation following stroke," *2007 IEEE 10th Int. Conf. Rehabil. Robot. ICORR'07*, vol. 0, no. c, pp. 896–901, 2007.

[12] M. Takagi, K. Iwata, Y. Takahashi, S. I. Yamamoto, H. Koyama, and T. Komeda, "Development of a grip aid system using air cylinders," *Proc. - IEEE Int. Conf. Robot. Autom.*, pp. 2312–2317, 2009.

[13] I. H. Ertas, E. Hocaoglu, D. E. Barkana, and V. Patoglu, "Finger exoskeleton for treatment of tendon injuries," *Proc. 11th IEEE Int. Conf. Rehabil. Robot. ICORR*, pp. 194–201, 2009.

[14] Y. Hasegawa, Y. Mikami, K. Watanabe, and Y. Sankai, "Five-fingered assistive

30

JMR-17-1307 (Design Innovation), Ben-Tzvi

hand with mechanical compliance of human finger," *Proc. - IEEE Int. Conf. Robot. Autom.*, pp. 718–724, 2008.

[15]   M. A. Zhou, P. Ben-Tzvi, and J. Danoff, "Hand rehabilitation learning system with an exoskeleton robotic glove," *IEEE Trans. Neural Syst. Rehabil. Eng.*, vol. PP, no. 99, pp. 1323–1332, 2015.

[16]   P. Ben-Tzvi, J. Danoff, and Z. Ma, "The Design Evolution of a Sensing and Force-Feedback Exoskeleton Robotic Glove for Hand Rehabilitation Application," *J. Mech. Robot.*, vol. 8, no. 5, p. 51019, May 2016.

[17]   P. Ben-Tzvi and Z. Ma, "Sensing and Force-Feedback Exoskeleton (SAFE) Robotic Glove," *IEEE Trans. Neural Syst. Rehabil. Eng.*, vol. 23, no. 6, pp. 992–1002, 2015.

[18]   Z. Ma and P. Ben-Tzvi, "An Admittance-Type Haptic Device - RML Glove," *ASME Int. Mech. Eng. Congr. Expo.*, pp. 1–7, 2011.

[19]   Z. Ma and P. Ben-Tzvi, "Design and Optimization of a Five-Finger Haptic Glove Mechanism," *J. Mech. Robot.*, vol. 7, no. 4, p. 41008, 2015.

[20]   H. In and K. Cho, "Exo-Glove : Soft wearable robot for the hand using soft tendon routing system," *IEEE Robot. Autom.*, vol. 22, no. March 2015, pp. 97–105, 2015.

[21]   S. W. Lee, K. A. Landers, and H. S. Park, "Development of a biomimetic hand exotendon device (BiomHED) for restoration of functional hand movement post-stroke," *IEEE Trans. Neural Syst. Rehabil. Eng.*, vol. 22, no. 4, pp. 886–898, 2014.

[22]   C. J. Nycz, M. A. Delph, and G. S. Fischer, "Modeling and design of a tendon actuated soft robotic exoskeleton for hemiparetic upper limb rehabilitation," *Proc. Annu. Int. Conf. IEEE Eng. Med. Biol. Soc. EMBS*, vol. 2015–Novem, pp. 3889–3892, 2015.

[23]   Y. Hasegawa, J. Tokita, K. Kamibayashi, and Y. Sankai, "Evaluation of fingertip force accuracy in different support conditions of exoskeleton," *Proc. - IEEE Int. Conf. Robot. Autom.*, pp. 680–685, 2011.

[24]   I. Koo, B. Byunghyun Kang, and K.-J. Cho, "Development of Hand Exoskeleton using Pneumatic Artificial Muscle Combined with Linkage," *J. Korean Soc. Precis. Eng*, vol. 11, no. 11, pp. 1217–1224, 2013.

[25]   P. Polygerinos, Z. Wang, K. C. Galloway, R. J. Wood, and C. J. Walsh, "Soft robotic glove for combined assistance and at-home rehabilitation," *Rob. Auton. Syst.*, vol. 73, pp. 135–143, 2015.

[26]   K. Tadano, M. Akai, K. Kadota, and K. Kawashima, "Development of grip amplified glove using bi-articular mechanism with pneumatic artificial rubber muscle," *Proc. - IEEE Int. Conf. Robot. Autom.*, pp. 2363–2368, 2010.

[27]   M. Liu and C. Xiong, "Synergistic characteristic of human hand during grasping tasks in daily life," *Lect. Notes Comput. Sci. (including Subser. Lect. Notes Artif. Intell. Lect. Notes Bioinformatics)*, vol. 8917, pp. 67–76, 2014.

[28]   W. E. Hook and J. K. Stanley, "Assessment of thumb to index pulp to pulp pinch

31

JMR-17-1307 (Design Innovation), Ben-Tzvi

grip strengths," *J. Hand Surg. Am.*, vol. 11, no. 1, pp. 91–92, 1986.

[29] K. Hemmi, K. and Inoue, "A Proposal of Three Dimensional Movement Model for Index Finger and Thumb," *Proc. 4th Asia-Pacific Conf. Control Meas.*, 2000.

[30] A. Hara, Y. Y. Amauchi, and K. Kusunose, "Analysis of Thumb and Index Finger Joints During Pinching Motion and Writing a Cross , as Measured by Electrogoniometers," *Clin. Biomech. Relat. Res.*, pp. 282–293, 1994.

[31] G. A. Bekey, R. Tomovic, and I. Zeljkovic, "Control architecture for the Belgrade/USC Hand," *Dexterous Robot. Hands*, p. 345, 1990.

[32] Z. Ma and P. Ben-Tzvi, "RML glove-an exoskeleton glove mechanism with haptics feedback," *IEEE/ASME Trans. Mechatronics*, vol. 20, no. 2, pp. 641–652, 2015.

[33] C. Yu and Q. Peng, "Robust recognition of checkerboard pattern for camera calibration," *Opt. Eng.*, vol. 45, no. 9, p. 93201, 2006.

[34] J. Pratt, B. Krupp, C. Morse, J. Pratt, and B. Krupp, "Feature Series elastic actuators for high fidelity force control," *Ind. Robot An Int. J.*, vol. 29, no. 3, pp. 234–241, 2002.

[35] M. Pratt, Gill; Williamson, "Series Elastic Actuators," *Proc. IEEE/RSJ Int. Conf. Intell. Robot. Syst.*, pp. 399–406, 1995.

32

JMR-17-1307 (Design Innovation), Ben-Tzvi

Figure Captions List

Fig. 1   Proposed design

Fig. 2   Anatomy of the human hand

Fig. 3   Design of the mechanism (a) Index finger, (b) Thumb (Both are shown for the left hand)

Fig. 4   Index mechanism showing two configurations and the design parameters for kinematic modelling. The relaxed configuration is shown in gray, while the black & white schematic shows a flexion configuration

Fig. 5   Simulation results (a) Desired index finger trajectory starting at the origin of (0, 0), (b) Index finger joint angles.

Fig. 6   Simulation results (a) Desired thumb trajectory starting at the origin of (0, 0), (b) Thumb joint angles.

Fig. 7   Design of the tip holder (same for thumb mechanism)

Fig. 8   System architecture of exoskeleton glove

Fig. 9   Experimental setup for the prototype: 1- Exoskeleton glove on mannequin, 2 - Embedded controller, 3 – Compressor, 4 - Air tank

Fig. 10   Experimental analysis at various stages of the bending motion: (a) Index finger, (b) Thumb

Fig. 11   Experimental results for (a) Index finger joints, (b) Thumb joints

Fig. 12   Prototype on a human hand: 1- Absolute position sensor, 2 - FSR sensor, 3 - Vibration motor, 4 - Pneumatic actuator

Fig. 13   Proposed SEA design

Fig. 14   3D printed prototype of SEA module

Fig. 15   Proposed Exo-Glove design with electric actuation and SEA

33

JMR-17-1307 (Design Innovation), Ben-Tzvi